APPLIED PHYSICS LETTERS 111, 022406 (2017); doi: 10.1063/1.4993433

Chopping skyrmions from magnetic chiral domains with uniaxial stress in magnetic nanowire

Yan Liu,[1] Na Lei,[2,3] Weisheng Zhao,[2,3] Wenqing Liu,[4] Antonio Ruotolo,[5] Hans-Benjamin Braun,[6,a)] and Yan Zhou[7,a)]

[1] *College of Sciences, Northeastern University, Shenyang 110819, People's Republic of China*

[2] *Fert Beijing Institute, Beihang University, Beijing 100191, China*

[3] *School of Electronic and Information Engineering, Beihang University, Beijing 100191, China*

[4] *Department of Electronic Engineering, Royal Holloway University of London, Egham, Surrey TW20 0EX, United Kingdom*

[5] *Department of Physics and Materials Science, City University of Hong Kong, Hong Kong, China*

[6] *UCD School of Physics, University College Dublin, Dublin, Ireland*

[7] *School of Science and Engineering, The Chinese University of Hong Kong, Shenzhen 518172, China*

ABSTRACT

Magnetic skyrmions are envisioned as ideal candidates as information carriers for future spintronic devices, which have attracted a great deal of attention in recent years. Due to their topological protection, the creation and annihilation of magnetic skyrmions have been a challenging task. Here, we numerically demonstrate that a magnetic skyrmion can be created by chopping a chiral stripe domain with a static uniaxial strain/stress pulse. This mechanism not only provides a method to create skyrmions in magnetic nanostructures but also offers promising routes for designing tunable skyrmionic-mechanic devices.

INTRODUCTION

Magnetic skyrmions are stable spin textures with the magnetic moments forming a twist structure, with the key characteristic that they are topological protected. After the first experimental discovery of magnetic skyrmions in MnSi [1], they have been observed in variety of magnetic systems, including B20-type materials with bulk Dzyaloshinskii-Moriya interaction (DMI) [1-7] and interfacial symmetry breaking multilayers with interfacial DMI [8-12]. Stability, small size and ultralow threshold current density for motion make the skyrmions very promising for future spintronic devices applications [13-19].

As information carriers, controllable creation of skyrmions is prerequisite for real application. The nucleation of isolated skyrmions is a challenging task as it necessarily involves overcoming the topological barrier, e.g. due to lattice discreteness effects [20]. Several different methods have been proposed to create individual skyrmions. They can be created by providing an external stimulus to a ferromagnetic state, such as applying a circulating current [21], injecting an in-plane, out-of-plane polarized current [13,22-24], using laser heating [25], or by spin waves [26]. In addition, skyrmions can be created by injecting an in-plane current into a notch [27] and be converted from a domain wall [28]. Very recently, Jiang *et al*. have shown experimentally that skyrmions can be generated by pushing chiral stripe domains (CSD) via a spin current through a geometrical constriction in heavy metal/ultrathin ferromagnet/insulator trilayers [29].

On the other hand, strain has been used to manipulate magnetic domains in soft magnetostrictive materials [30-35]. Recent, experiments have demonstrated that mechanical strain or stress are effective means to control the skyrmion phase [36-38]. In this letter, we

will show that it is possible to cut a skyrmion from a chiral stripe domain (CSD) by applying an in-plane uniaxial strain. It is well known that the application of a static uniaxial strain to a magnetostrictive material can induce an additional uniaxial anisotropy to the magnetic energy [32]. The resulting magneto-elastic anisotropy field can be expressed as

$$\mathbf{H}_{strain} = -3\varepsilon_i E\lambda(\mathbf{m}\cdot\hat{\mathbf{n}}_s)\hat{\mathbf{n}}_s \quad (1)$$

where ε_i is the uniaxial strain with i=x, y, $\hat{\mathbf{n}}_s$ is the direction of the strain, E is the Young's modulus, $\mathbf{m}$ is the unit vector of the magnetization, and λ is the magnetostriction constant. This effective field acts on the CSD, modifies the magnetic free energy and leads to a reorientation of the magnetization. Figure 1(a)-(c) schematically shows the mechanism of evolution of a Néel CSD to a skyrmion under a uniaxial strain along the x axis. The in-plane component of the magnetization in CSD is mainly along the y-axis. In contrast, the magneto-elastic anisotropy field is along the x axis (Fig. 1(a)). Thus, $\mathbf{H}_{strain}$ drags the magnetizations to rotate to the x axis, which gradually forms a bottleneck area at the place near that domain end (Fig. 1(b)). If the strain is large enough, the strain anisotropy energy is larger than the elastic energy, the CSD will break at the bottleneck area, which results in a circular domain breaking off from the CSD, and finally it evolves to a skyrmion (Fig. 1(c)). A similar mechanism can be realized in a Bloch CSD by applying a uniaixal strain along the y direction (Fig. 1(d)-(f)).

MODEL

To demonstrate the aforementioned idea, we study the geometry as shown in Fig. 2 for generating skyrmions by an in-plane uniaxial strain. The sample we considered is a 1.1-nm-thick ferromagnetic nanostripe with a width of 120 nm and a length of 1000 nm with

a geometrical constriction at the center. The length and width of the constriction are fixed to be 100 nm and 82 nm, respectively. We assume that the DMI in the ferromagnetic layer is either of bulk or interfacial type, which will generate Bloch and Néel skyrmions respectively. The left region of the sample (chiral stripe region) initially supports a CSD, while the ferromagnetic background is presented at the right region (skyrmion region). The CSD can be injected into the left hand part by injecting an in-plane current. The constricted region in the center (strain region) is attached to the commonly used piezoelectric material $Pb(Zr,Ti)O_3$ (PZT). A perpendicular magnetic field H_z is applied to the whole sample. The PZT is polarized along x-direction for interfacial type (Fig. 2(a)) and y-direction for bulk type (Fig. 2(b)). By applying a voltage to the PZT, an in-plane uniaxial piezostrain is induced, and then this piezostrains is transferred to the ferromagnetic layer. This strain transfer from a PZT layer to ferromagnetic layers have been experimentally demonstrated in many works [33,39-40]. Here, the in-plane uniaxial piezostrain is assumed to be uniform in the strain region, and vanishing outside this region. The strain is directed along the x-direction for the ferromagnet with interfacial DMI, and along the y-direction for the ferromagnet with bulk DMI. In addition to the strain, an in-plane spin-polarized current is applied to drive the CSD or the skyrmions to move forward. The geometrical constriction in the strain region is set for restricting the CSD in the chiral stripe region without expanding it into the skyrmion region.

METHOD

The study is carried out by means of public object-oriented micromagnetic framework (OOMMF) code [41]. The time-dependent magnetization dynamics is governed by the Laudau-Lifshitz-Gilbert (LLG) equation,

$$\frac{d\mathbf{m}}{dt} = -|\gamma|\mathbf{m}\times\mathbf{H}_{eff} + \alpha\left(\mathbf{m}\times\frac{d\mathbf{m}}{dt}\right), \tag{2}$$

where γ is the gyromagnetic ratio, and α is the Gilbert damping constant. The effective magnetic field is given by $\mathbf{H}_{\text{eff}} = -1/(\mu_0 M_s)(\partial W/\partial \mathbf{m})$, where μ_0 is the vacuum permeability, and W is the magnetic energy of the system consisting of exchange, anisotropy, Dzyaloshinskii-Moriya interaction (DMI) [42], and strain-induced anisotropy energy terms. The DMI interaction is assumed to be of bulk or interfacial origin. The bulk DMI energy density is given by $w_{\text{DM}} = D\mathbf{m}\cdot(\nabla\times\mathbf{m})$, where D is the DM interaction constant. The interfacial DMI energy density is $w_{\text{DM}} = -D\mathbf{m}\cdot((\hat{\mathbf{z}}\times\nabla)\times\mathbf{m})$. The strain-induced anisotropy energy, which originates from the uniaxial strain applied to the film, can be written as [34]

$$W_{strain} = -\frac{3}{2}\varepsilon_i E\lambda(\mathbf{m}\cdot\hat{\mathbf{n}}_s)^2 \tag{3}$$

For simulation of the current in-plane injection to the nanostripe, the spin-transfer torque (STT) including both adiabatic and non-adiabatic terms was added to Eq. (2), with

$$\tau_{\text{STT}} = \mu\mathbf{m}\times(\frac{\partial\mathbf{m}}{\partial x}\times\mathbf{m}) + \beta\mu(\frac{\partial\mathbf{m}}{\partial x}\times\mathbf{m}) \tag{4}$$

where $\mu = \mu_B JP/eM_s$, M_s is the saturation magnetization, J is the current density, P is the spin polarization, μ_B is Bohr magneton, e is the electron charge, and β is the non-adiabaticity factor. Because the constriction of the strain region, the current density is inhomogeneous. The current density we mentioned in this paper is the current density in the wide region, and the current density in the strain region is $J_s = JW/W_1$, where J is the current density in the wide region, W and W_1 are the width of the wide region and the strain region, respectively.

Material parameters used for the simulations are set to represent $Co_{20}Fe_{60}B_{20}$. According to

the measurement results in Ref. 29, we use the following parameters: A saturation magnetization of $M_s = 6.5\times10^5$ A/m, an exchange constant $A = 4.8\times10^{-12}$ J/m, and a perpendicular anisotropy constant $K_u = 2.3\times10^4$ J/m^3. In this work we set the DMI constant to $D = 1.0\times10^{-3}$ J/m^2. From Ref. 43, we have $\lambda = 31$ ppm and $E = 1.6\times10^{11}$ J/m^3. The sample is discretized into small cells with a cell size of $2\times2\times1.1$ nm^3, the Gilbert damping constant is $\alpha = 0.1$, the non-adiabaticity factor $\beta = 0.1$, and the degree of spin polarization is P=0.5.

It should be mentioned that the demagnetization energy or the magnetic dipole interaction is neglected in our model. In thin-plate magnets, magnetic skyrmions is often realized by competition among the magnetostatic energy, the exchange interaction, and the uniaxial magnetic anisotropy [44-47]. For our model, comparing the results of with and without including the demagnetization energy, the influence of the demagnetization energy approximately reduces to a perpendicular uniaxial anisotropy with anisotropy constant $K_{eff} = 0.5\mu_0 M_s^2$. Therefore, the demagnetization energy only quantitatively affects our results without any qualitative changes.

SIMULATION RESULTS

Figure 3(a) shows the Néel skyrmion generation process via application of a strain pulse to a CSD [see also Multimedia view]. The CSD at the chiral stripe region is firstly driven to the strain region by the in-plane current (t=0-2.5 ns). At t=2.5 ns, a uniaxial strain ε_x along the x direction is applied. Under the effect of the strain, the right end of CSD bends upwards, forming a depression in the bending region (t=3.0 ns). The width of the CSD in the bending region is gradually compressed, and then a small domain breaks down from the CSD (t=3.5

ns). Subsequently, the small domain evolves to a skyrmion (t=4.1 ns). For demonstration of the application of strain-induced skyrmion generation in the nanostripe with bulk DMI, we use the same parameters to simulate the Bloch skyrmion generation process. Figure 3(d) shows the Bloch skyrmion generation process by applying an uniaxial strain along the y direction [see also Multimedia view]. The process is similar to the case of Neel skyrmion generation. The generation of a skyrmion can also be confirmed by analyzing the topological number of the system. In a planar system, the topological number of the system is given by $S=\frac{1}{4\pi}\sum_{x,y} q(x,y)$, where $q(x,y)=\mathbf{m}\cdot(\partial_x\mathbf{m}\times\partial_y\mathbf{m})$ is the topological density of the cell with coordinate (x, y). Figure 3(b) shows the development of S. Before applying the strain, the value of S is 0.5, which is the topological number of the half skyrmion at the right end of CSD. At t=3.5 ns, S suddenly increases to about 1.5. This increment indicates that one skyrmion is created.

We have confirmed that both Néel and Bloch skyrmion can be created by cutting CSD with an uniaxial strain. However, we are interested in the detailed dynamical process to understand how a skyrmion is created. Figure 4 shows the temporal evolution of the topological density and energy density together with magnetization profile within the dashed square in Fig. 3(a). After the strain is switched on, like a uniaxial anisotropy along x direction acting on the magnetizations, the magnetizations rotates towards the x axis. This causes the half skyrmion at the right end of the CSD to bends upward, which induces the formation of a topological 'dip' in the bending region (t=3.1 ns). The topological density of the 'dip' is negative and increases gradually. With the development of the 'dip', a small domain is gradually separated from the CSD. At t=3.47 ns, the small domain breaks off from the CSD. Interestingly, the

small domain has a peculiar spin structure with a topological number equivalent to zero. One end of it is a half skyrmion, and the other end is a half anti-skyrmion. The chirality of the half skyrmion is favored by the DMI, while the half anti-skyrmion is unfavored by the DMI which increases the energy (indicated by the green region). Thus, the magnetizations tends to be oriented towards the direction favored by the DMI, which causes the half anti-skyrmion to be compressed into a small region that concentrates a large amount of energy [t=3.47-3.564 ns]. At t=3.564 ns, the size of the half anti-skyrmion is compressed to be comparable to a Bloch point in a classical bubble material, and the topological density of this area reverses under emission of spin waves (t=3.564-3.586 ns), which switches the half anti-skyrmion to a half skyrmion. The switching increases the topological number of the small domain to 1 that corresponds to the topological number of a single skyrmion, in which the spins wrap once around a unit sphere [20]. Finally, the small domain eventually evolves to be a proper skyrmion (t=3.6 ns). The switching from a half anti-skyrmion to a half skyrmion is accompanied by a change in topological charge, which increases by an integer $\Delta S = 1$. In general, the mechanism of a $\Delta S = 1$ topological change entails the formation of a singularity in the continuum limit. In thick materials, it evolves the injection and propagation of a Bloch point vertically through the finite thickness of the sample. In two-dimensional samples, a Bloch point cannot exist, an equivalent process has been mentioned [13, 19, 48], where the singularity is simply formed by four neighboring moments, the "injection and propagation" of the singularity then simply amounts to the collective switching of typically three neighboring moments from plus to minus orientation [13]. In our case, the nanostripe is just 1.1 nm thick, and it can be treated effectively as a two-dimensional thin film. So the switching from a half

anti-skyrmion to a half skyrmion is similar as the process in Ref. 13, which evolves "injection and propagation" of the singularity.

For this skyrmion generation mechanism, current density and strain are two important factors. Figure 5 shows a final phase diagram after applying a 3-ns pulse of strain on the strain region. There exists a threshold current J_s =40 MA/cm^2 and a threshold strain ε_s =0.67% for generating skyrmions from a CSD. Below this threshold current, the CSD stays at the strain region or is even forced to return to the chiral stripe region. However, too large a current forces the half skyrmion at the end of the CSD to move too quickly such that the CSD extends to the skyrmion region without being cut. When the strain is below the threshold value, the forces acting on the CSD from the stain are not sufficient to cut a small domain off the CSD. In contrast too large strain may force the CSD to return to the chiral stripe region. Also, the shape of the strain pulse influences the generation of the skyrmion. If the strain pulse duration is too short, the cutting process cannot be finished, so the skyrmion cannot be generated. If the strain pulse duration is long enough, the skyrmion can be created one by one.

CONCLUSION

Our results have demonstrated that uniaxial strain can be an effective way to generate skyrmions of both Néel and Bloch type. This intriguing approach provides a mechanism to generate skyrmions. In the future, it could be used in advanced skyrmionic device, for example, skyrmion racetrack memory.

ACKNOWLEDGMENTS

Y.Z. acknowledges support by the National Natural Science Foundation of China (Project No.

1157040329, No. 11404053, No. 11274261) and Shenzhen Fundamental Research Fund under Grant No. JCYJ20160331164412545.

REFERENCES

[1] S. Mühlbauer, B. Binz, F. Jonietz, C. Pfleiderer, A. Rosch, A. Neubauer, R. Georgii, and P. Böni, Science **323**, 915 (2009).

[2] X. Z. Yu, Y. Onose, N. Kanazawa, J. H. Park, J. H. Han, Y. Matsui, N. Nagaosa, and Y. Tokura, Nature **465**, 901 (2010).

[3] X. Z. Yu, N. Kanazawa, Y. Onose, K. Kimoto, W. Z. Zhang, S. Ishiwata, Y. Matsui, and Y. Tokura, Nat. Mater. **10**, 106 (2011).

[4] K. Shibata, X. Z. Yu, T. Hara, D. Morikawa, N. Kanazawa, K. Kimoto, S. Ishiwata, Y. Matsui, and Y. Tokura, Nat. Nanotechnol. **8**, 723 (2013).

[5] C. Franz, F. Freimuth, A. Bauer, R. Ritz, C. Schnarr, C. Duvinage, T. Adams, S. Blügel, A. Rosch, Y. Mokrousov, and C. Pfleiderer, Phys. Rev. Lett. **112**, 186601 (2014).

[6] Y. Tokunaga, X. Z. Yu, J. S. White, H. M. Rønnow, D. Morikawa, Y. Taguchi, and Y. Tokura, Nat. Commun. **6**, 7638 (2015).

[7] T. Tanigaki, K. Shibata, N. Kanazawa, X. Yu, Y. Onose, H. S. Park, D. Shindo, and Y. Tokura, Nano Lett. **15**, 5438 (2015).

[8] S. Heinze, K. von Bergmann, M. Menzel, J. Brede, A. Kubetzka, R. Wiesendanger, G. Bihlmayer, and S. Blügel, Nat. Phys. **7**, 713 (2011).

[9] A. Sonntag, J. Hermenau, S. Krause, and R. Wiesendanger, Phys. Rev. Lett. **113**, 077202 (2014).

[10] C. Moreau-Luchaire, C. Moutafis, N. Reyren, J. Sampaio, C. A. F. Vaz, N. Van Horne1, K. Bouzehouane, K. Garcia, C. Deranlot, P. Warnicke, P. Wohlhüter, J. -M. George, M. Weigand, J. Raabe, V. Cros, and A. Fert, Nat. Nanotechnol. **11**, 444 (2016).

[11] O. Boulle, J. Vogel, H. Yang, S. Pizzini, D. de S. Chaves, A. Locatelli, T. O. Mente, A. Sala, L. D. Buda-Prejbeanu, O. Klein, M. Belmeguenai, Y. Roussigné, A. Stashkevich, S. M. Chérif, L. Aballe, M. Foerster, M. Chshiev, S. Auffret, I. M. Miron, and G. Gaudin, Nat. Nanotechnol. **11**, 449 (2016).

[12] G. Chen, A. Mascaraque, A. T. N'Diaye, and A. K. Schmid, Appl. Phys. Lett. **106**, 242404 (2015).

[13] J. Sampaio, V. Cros, S. Rohart, A. Thiaville, and A. Fert, A. Nat. Nanotechnol. **8**, 839 (2013).

[14] R. Tomasello, E. Martinez, R. Zivieri, L. Torres, M. Carpentieri, and G. Finocchio, Sci. Rep. **4**, 6784 (2014).

[15] X. Zhang, G. P. Zhao, H. Fangohr, J. Ping Liu, W. X. Xia, J. Xia, and F. J. Morvan, Sci. Rep. **5**, 7643 (2015).

[16] X. Zhang, M. Ezawa, and Y. Zhou, Sci. Rep. **5**, 9400 (2015).

[17] Y. Liu, H. F. Du, M. Jia, and A. Du, Phys. Rev. B **91**, 094425 (2015).

[18] F. Ma, Y. Zhou, H. B. Braun, and W. S. Lew, Nano Lett. **15**, 4029 (2015).

[19] Y. Zhou, E. Iacocca, A. A. Awad, R. K. Dumas, F. C. Zhang, H. B. Braun, and J. Äkerman, Nat. Commun. **6**, 8193 (2015).

[20] H. -B. Braun, Adv. Phys. **61**, 1 (2012).

[21] Y. Tchoe and J. H. Han, Phys. Rev. B **85**, 174416 (2012).

[22] N. Romming, C. Hanneken, M. Menzel, J. E. Bickel, B. Wolter, K. von Bergmann, A. Kubetzka, and R. Wiesendanger, Science **341**, 636 (2013).

[23] S. -Z. Lin, C. Reichhardt, and A. Saxena, Appl. Phys. Lett. **102**, 222405 (2013).

[24] G. Yin, Y. Li, L. Kong, R. K. Lake, C. L. Chien, and J. Zang, Phys. Rev. B **93**, 174403 (2016).

[25] W. Koshibae and N. Nagaosa, Nat. Commun. **5**, 5148 (2014).

[26] Y. Liu, G. Yin, J. Zang, J. Shi, and R. K. Lake, Appl. Phys. Lett. **107**, 152411 (2015).

[27] J. Iwasaki, M. Mochizuki, and N. Nagaosa, Nat. Nanotechnol. **8**, 742 (2013).

[28] Y. Zhou and M. Ezawa, Nat. Commun. **5**, 4652 (2014).

[29] W. Jiang, P. Upadhyaya, W. Zhang, G. Yu, M. B. Jungfleisch, F. Y. Fradin, J. E. Pearson, Y. Tserkovnyak, K. L. Wang, O. Heinonen, S. G. E. te Velthuis, and A. Hoffmann, Science **349**, 283 (2015).

[30] D. E. Parkes, S. A. Cavill, A. T. Hindmarch, P. Wadley, F. McGee, C. R. Staddon, K. W. Edmonds, R. P. Campion, B. L. Gallagher, and A. W. Rushforth, Appl. Phys. Lett. **101**, 072402 (2012).

[31] D. E. Parkes, S. A. Cavill, A. T. Hindmarch, P. Wadley, F. McGee, C. R. Staddon, K.W. Edmonds, R. P. Campion, B. L. Gallagher, and A.W. Rushforth, Appl. Phys. Lett. **102**, 032405 (2013).

[32] J. V. Jäger, A. V. Scherbakov, T. L. Linnik, D. R. Yakovlev, M. Wang, P. Wadley, V. Holy, S. A. Cavill, A. V. Akimov, A. W. Rushforth, and M. Bayer, Appl. Phys. Lett. **103**, 032409 (2013).

[33] N. Lei, T. Devolder, G. Agnus, P. Aubert, L. Daniel, J. -V. Kim, W. Zhao, T. Trypiniotis, R. P. Cowburn, C. Chappert, D. Ravelosona, and P. Lecoeur, Nat. Commun. **4**, 1378 (2013).

[34] T. A. Ostler, R. Cuadrado, R.W. Chantrell, A.W. Rushforth, and S. A. Cavill, Phys. Rev. Lett. **115**, 067202 (2015).

[35] J. -M. Hu, T. Yang, K. Momeni, X. Cheng, L. Chen, S. Lei, S. Zhang, S. Trolier-McKinstry, V. Gopalan, G. P. Carman, C. -W. Nan, and L. Q. Chen, **16**, 2341 (2016).

[36] K. Shibata, J. Iwasaki, N. Kanazawa, S. Aizawa, T. Tanigaki, M. Shirai, T. Nakajima, M. Kubota, M. Kawasaki, H. S. Park, D. Shindo, N. Nagaosa1, and Y. Tokura, Nat. Nanotechnol. **10**, 589 (2015).

[37] Y. Nii, T. Nakajima, A. Kikkawa, Y. Yamasaki, K. Ohishi, J. Suzuki, Y. Taguchi, T. Arima, Y. Tokura, and Y. Iwasa, Nat. Commun. **6**, 8539 (2015).

[38] H. C. Wu, K. D. Chandrasekhar, T. Y. Wei, K. J. Hsieh, T. Y. Chen, H. Berger, and H. D. Yang, J. Phys. D: Appl. Phys. **48**, 475001 (2015).

[39] D. E. Parkes, S. A. Cavill, A. T. Hindmarch, P. Wadley, F. McGee, C. R. Staddon, K. W. Edmonds, R. P. Campion, B. L. Gallagher, and A. W. Rushforth, Appl. Phys. Lett. **101**, 072402 (2012).

[40] S. A. Cavill, D. E. Parkes, J. Miguel, S. S. Dhesi, K. W. Edmonds, R. P. Campion, and A. W. Rushforth, Appl. Phys. Lett. **102**, 032405 (2013).

[41] M. Donahue and D. G. Porter, OOMMF User's guide, Version 1.0, Interagency Report NISTIR 6376, NIST, Gaithersburg, MD, 1999.

[42] A. N. Bogdanov and U. K. Rößler, Phys. Rev. Lett. **87**, 037203 (2001).

[43] D.Wang, C. Nordman, Z. Qian, J. M. Daughton, and J. Myers, J. Appl. Phys. **97**, 10C906 (2005).

[44] M. Beg, R. Carey, W. Wang, D. Cortés-Ortuño, M. Vousden, M. Bisotti, M. Albert, D. Chernyshenko, O. Hovorka, R. L. Stamps, and H. Fangohr, Sci. Rep. **5**, 17137 (2015).

[45] R. Carey, M. Beg, M. Albert, M. Bisotti, D. Cortés-Ortuño, M. Vousden, W. Wang, O. Hovorka, and H. Fangohr, Appl. Phys. Lett. **109**, 122401 (2016).

[46] M. Vousden, M. Albert, M. Beg, M. Bisotti, R. Carey, D. Chernyshenko, D. Corté s-Ortuño, W. Wang, O. Hovorka, C. H. Marrows, and H. Fangohr, Appl. Phys. Lett. **108**, 132406 (2016).

[47] M. Beg, M. Albert, M. Bisotti, D. Cortés-Ortuño, W. Wang, R. Carey, M. Vousden, O. Hovorka, C. Ciccarelli, C. S. Spencer, C. H. Marrows, and Hans Fangohr, Phys. Rev. B **95**, 014433 (2017).

[48] C. Heo, N. S. Kiselev, A. K. Nandy, S. Blügel, and T. Rasing, Sci. Rep. **6**, 27146 (2016).

Figures

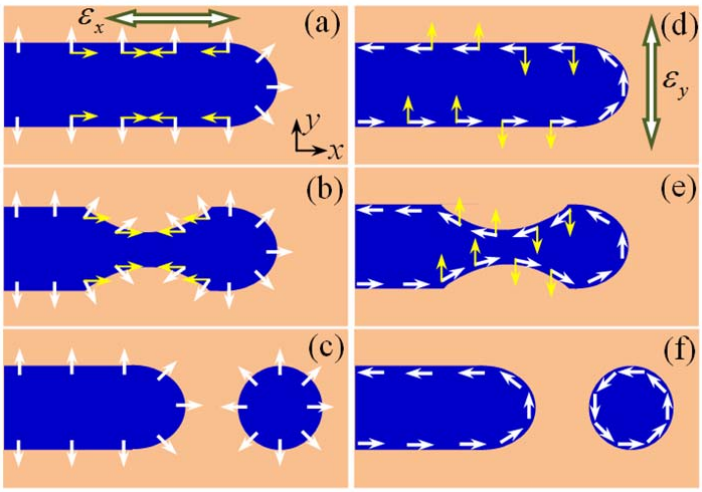

Figure 1 Schematic of the cutting effect of a static uniaxial strain on a CSD and the formation of a skyrmion. (a-c) Evolution of a Néel CSD under a uniaxial strain ε_x. The blue region is a CSD, and the light orange region is the ferromagnetic background. The white arrows show the in-plane magnetization direction of the CSD. The yellow arrows show the direction of the effective strain anisotropy field. (d-f) Evolution of a Bloch CSD under a static uniaxial strain ε_y.

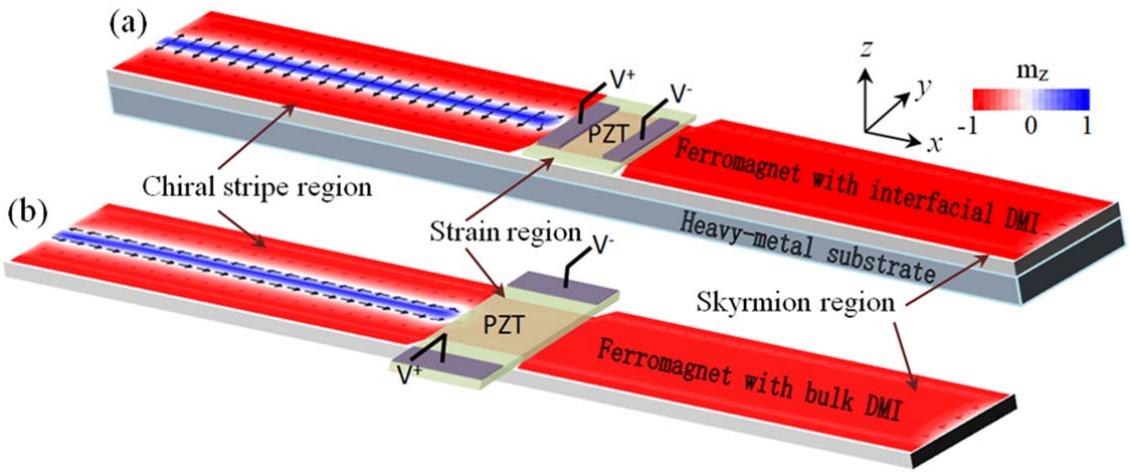

Figure 2 Design of the skyrmion generation device. (a) Néel skyrmion generation in a ferromagnet/heavy metal bilayers system, where the interfacial symmetry breaking introduces the interfacial DMI. (b) Bloch skyrmion generation in a ferromagnetic layer with bulk DMI. The arrows represent the in-plane component of the magnetization and the colors encode the *z* component. The color-scale has been used throughout this paper.

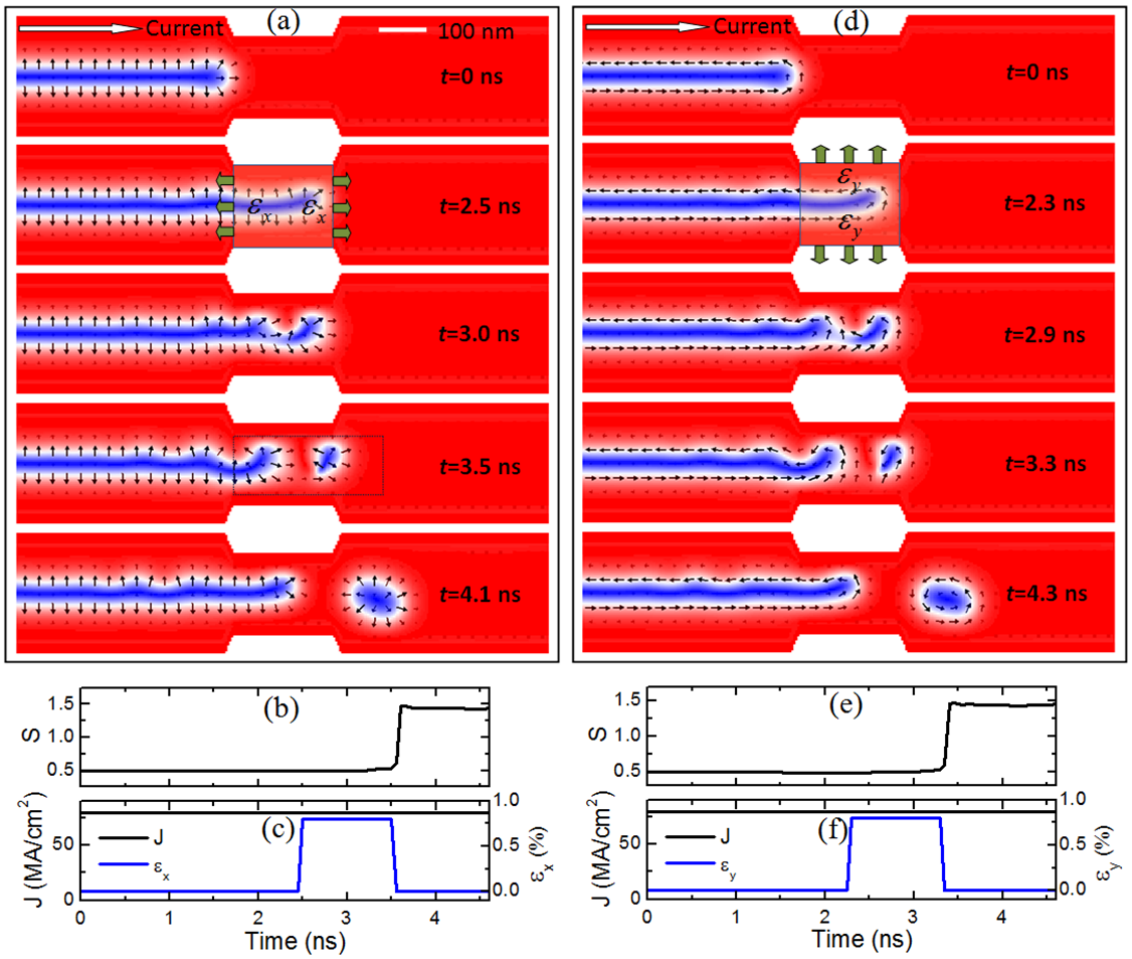

Figure 3 The magnetization evolution of the skyrmion generation is obtained by applying a strain pulse and an in-plane current with current density J =80 MA/cm^2, where H_z=70 mT. (a-c) A Néel skyrmion is generated by applying a 1 ns-duration strain pulse ε_x with strength of 0.8 % at t=2.5 ns. (Multimedia view) [URL:] (d-e) A Bloch skyrmion is generated by applying a 1 ns-duration strain pulse ε_y with strength of 0.8 % at t=2.3 ns. (Multimedia view) [URL:] (a) and (d) show the snapshots of the magnetization configuration at the indicated times. (b) and (e) show the time evolution of the topological number S. (c) and (f) show the in-plane current and strain pulse applied during the simulation.

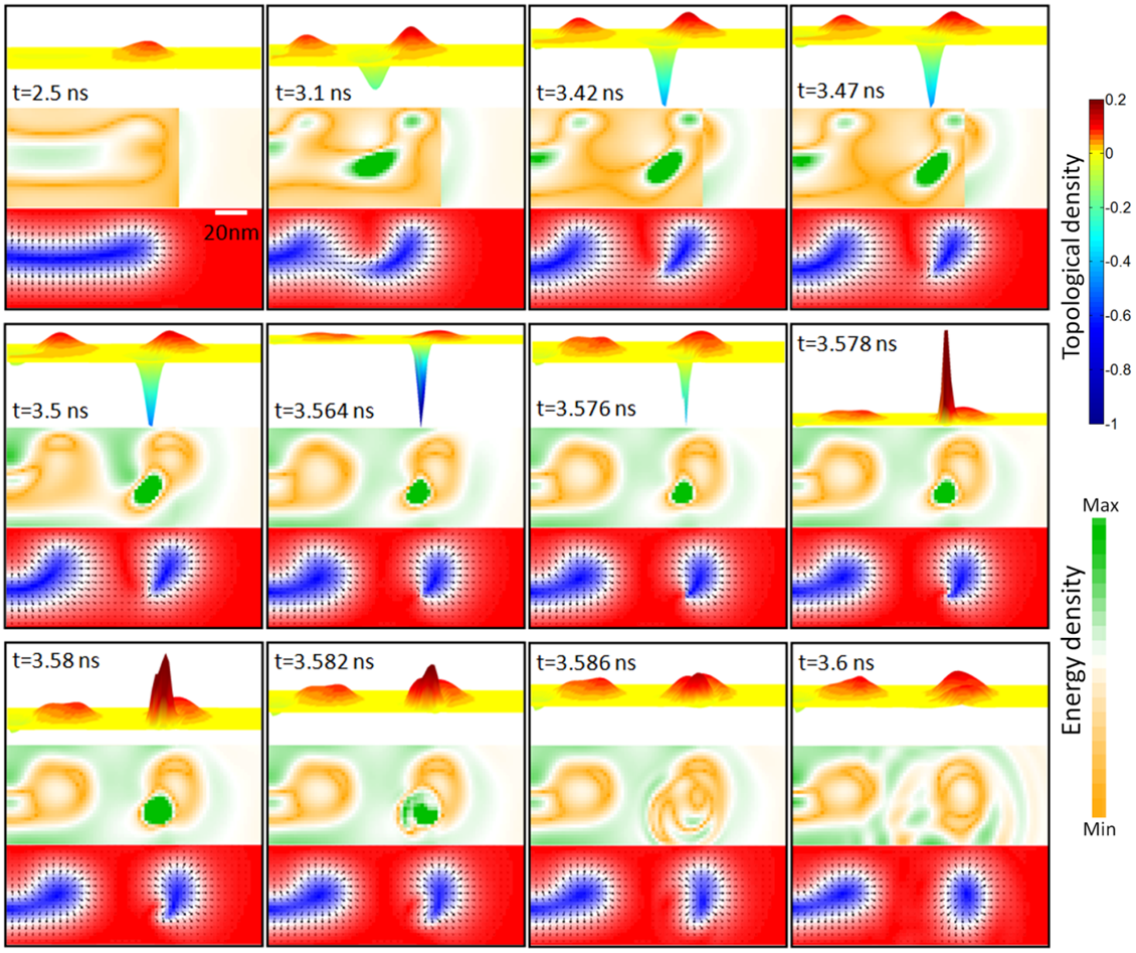

Figure 4 Detailed dynamics of skyrmion generation. The top panels display the snapshot images of the topological density within the dashed square in Fig. 2(a) taken at the indicated times from the perspective views. The middle panels show the corresponding energy density, and the bottom panels present the corresponding top view of the magnetization distribution. (Multimedia view) [URL:]

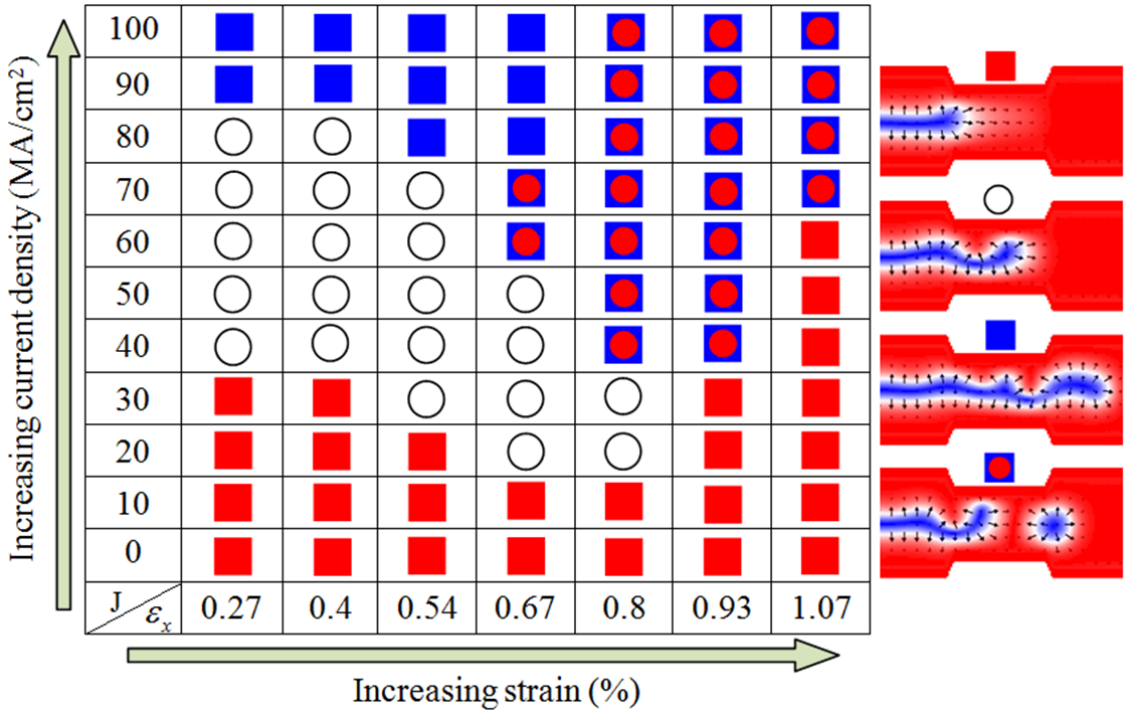

Figure 5 Effect of the current and strain on the magnetization dynamics. Left panel shows the final phase diagram after applying a 3-ns pulse of strain on the strain region, where the current are always turned on, and H_z=70 mT. Four different end states are identified (right panel): the CSD is forced to go back to the chiral stripe region (red square), the CSD stays at the strain region (hollow circle), the CSD moves to the skyrmion region without being cut (blue square), and skyrmion form (blue square with red circle).